Major histocompatibility complex class II-expressing bone marrow megakaryocytes activate CD4$^+$ T cells and induce regulatory T cell fate

Virginia Camacho[1,2], Karen G. Wang†[1], Pavel Hanč[3], Estelle Carminita[1,2], Isabelle C. Becker[1,2], Dong H. Lee[1], Marcelo Falchetti[4], Jaxaira Maggi[5], Maria Barrachina[1,2], Ulrich von Andrian[3,6], Montserrat Carrascal[5], Joseph E. Italiano[1,2], and Kellie R. Machlus*[1,2]

1. Vascular Biology Program, Boston Children's Hospital, Boston, MA, USA.
2. Department of Surgery, Harvard Medical School, Boston, MA, USA.
3. Department of Immunology, Harvard Medical School, Boston, MA, USA.
4. Department of Biological Chemistry and Molecular Pharmacology, Harvard Medical School, Boston, MA, USA.
5. Biological and Environmental Proteomics Group, Institute of Biomedical Research of Barcelona, Spanish National Research Council (IIBB-CSIC/IDIBAPS), Barcelona, Spain.
6. The Ragon Institute of Massachusetts General Hospital (MGH), Massachusetts Institute of Technology (MIT) and Harvard, Cambridge, MA, USA.

†Present address: Perelman School of Medicine, University of Pennsylvania, Philadelphia, PA, USA.

*Corresponding author
Kellie Machlus, PhD
Kellie.Machlus@childrens.harvard.edu
Karp Family Research Building
1 Blackfan Circle, Room 11.214
Boston, MA 02115

Abstract

While professional antigen-presenting cells drive adaptive immunity, atypical cell types can fulfill this role in the bone marrow. Megakaryocytes (MKs) are canonically recognized for platelet production, but recent studies indicate functional heterogeneity and immune potential. We found that ~20% of bone marrow MKs express Major Histocompatibility Complex (MHC) II and co-stimulatory receptors CD80, CD86, and CD40. These MKs process and present antigen to activate T cells in an MHC II–dependent manner. MK–T cell interactions induced TGF-β1 secretion and promoted induced regulatory T cell differentiation. Immunopeptidomics of MK MHC II receptor confirmed occupancy by exogenous peptides, demonstrating in vivo functionality. Using a model with MK-targeted deletion of MHC II (*Pf4-MHC*$^{\Delta/\Delta}$ mice), we observed altered TLR signaling, reduced bone marrow TGF-β1, and decreased numbers of hematopoietic stem cells. Together, these findings identify MHC II+ MKs as noncanonical antigen-presenting cells that modulate adaptive immunity and maintain the hematopoietic niche.

One Sentence Summary: MHC II-positive megakaryocytes present antigen, express co-stimulatory receptors, and activate CD4^{+} T cells.

INTRODUCTION

Megakaryocytes (**MKs**) are large (50–100 µm) bone marrow cells derived from hematopoietic stem cells (**HSCs**), recognized for the ability to generate platelets. Platelets are circulating cells essential for blood clotting and wound healing (1). MKs also have an established role in regulating hematopoiesis. This is partially executed via cytokine release; MKs produce TGF-β1 and CXCL4, which help maintain HSC quiescence in vivo (2, 3). MKs also support HSC niche remodeling, including osteoblast expansion, following radiation injury (4, 5), and promote HSC proliferation under stress conditions by producing FGF1 and IGF-1 (6, 7). The spatial positioning of MKs next to HSCs not only regulates HSC activity but also influences lineage output; HSCs adjacent to MKs exhibit a greater platelet- and myeloid-biased differentiation profile compared to HSCs in other marrow regions, such as the arteriolar niche. Furthermore, MK depletion can reprogram these myeloid-biased HSCs toward a more lineage-balanced state (8). Thus, MKs are established regulators of the bone marrow microenvironment.

Recent single cell analyses of human and murine bone marrow MKs have revealed transcriptional heterogeneity within this population and demonstrate that MKs have spatially and functionally specialized roles within this niche (9-11). As such, the range of functions attributed to MKs has expanded, evolving from terminally differentiated, short-lived polyploid cells principally involved in platelet production, to cells that play roles in HSC support, bone marrow niche regulation, and the instruction of adaptive immunity. Four major MK subsets have been described including an 'immune-MK' based on the enrichment of genes associated with antigen presentation and TLR signaling (9, 11). This supports the notion that MKs in the marrow harbor immunomodulatory potential, as has been described in tissues such as the lung and spleen (12, 13).

The presentation of peptides by antigen presenting cells (**APCs**) is a key driver in the initiation and regulation of adaptive immunity. Major Histocompatibility Complex (**MHC**) class I is found on all nucleated cells and presents antigenic peptides to CD8+ T cells. Conversely, constitutive MHC class II expression is restricted to 'professional APCs'. While dendritic cells are regarded as the typical professional APC of the immune system, dendritic cells are not solely responsible for priming CD4+ T cell responses. Atypical cell types can execute this role in tissues such as the bone marrow with a unique immunological profile (14-16). In the bone marrow, HSCs can process and present antigen via MHC II (17). This safeguards HSCs from exhaustion and prevents malignant transformation. Furthermore, in HSCs, MHC II expression increases with age, and these MHC II+ aged HSCs are found more proximal to regulatory T cells (**Tregs**). Specifically, the interaction between MHC II+ HSCs and Tregs helps aged HSCs maintain long-term survival by creating an environment that limits the effects of inflammation and immune attack (18). This expands on other studies demonstrating that bone marrow Tregs directly and indirectly support the maintenance and function of HSCs, as well as the stromal microenvironment via IL-10 (18, 19). Together, these studies support the notion of CD4+ T cell crosstalk with hematopoietic cells in the bone marrow to regulate hematopoiesis.

In this manuscript, we characterize MHC II-expressing MKs in the bone marrow. We confirmed the presence of MHC II on a subset of bone marrow MKs in both mice and humans. Notably, MHC II was absent in platelets, even when activated, suggesting that while MKs express this molecule, they do not transfer it to platelets. We observed that stimulation of MKs with TLR agonists such as poly I:C and LPS enhanced the expression of MHC II and co-stimulatory molecules, indicating functional TLR responses. Bone marrow MKs harbored the ability to activate $CD4^+$ T cells in an MHC II-dependent manner ex vivo. Further, transcriptomic profiling of MHC II+ MKs revealed upregulated interferon responses and enhanced phagocytic capacity. Finally, MK-specific deletion of MHC II *(Pf4-MHC*$^{\Delta/\Delta}$ mice) altered MK responsiveness to TLR agonists in vivo, reduced bone marrow TGF-β1 production, and altered stem and progenitor cell responses to TLR stimulation in the bone marrow. Overall, this work highlights a key role for MHC II+ MKs as regulators in the bone marrow via MHC II mediated $CD4^+$ T cell activation.

RESULTS

MHC II is expressed throughout the megakaryocyte lineage

To characterize the MHC II expression in the myelo-erythroid progenitor populations in the bone marrow, we utilized a murine MHC II–EGFP knock-in model, in which green fluorescent protein (**EGFP**) is fused to the MHC II beta chain and expression is driven by endogenous transcriptional activity (20, 21). This model provided a tool for identifying MHC II expressing cells while limiting potential artifacts associated with antibody-based labeling approaches. Using MHC II–EGFP knock-in mice, we compared the MHC II across various stem and progenitor populations in the bone marrow. These data revealed that MHC II expression was prevalent in the MK lineage; 17.7% ± 5.07 (mean ± SD) of mature MKs (Lineage- CD41+ CD42d+) expressed MHC II (**Fig 1A-B**). Further, approximately 39% (± 15.74) of MkPs (CD150+ CD41+ Lineage-Sca-1-c-kit+) expressed MHC II (**Fig 1A-B** and **S1A-B**) and intriguingly, MK biased HSCs were also enriched in MHC II expression (57.4 ± 21.6, **Fig 1A, C**). MK-erythroid progenitors expressed low amounts of MHC II, with expression decreasing along the erythroid lineage and reappearing in granulocyte-monocyte progenitors (**Fig 1C, S1A**). MHC II expression was also visualized using high-dimensional flow cytometry, displaying its co-expression with CD41+ MKs and MK progenitor cells (**Fig 1D**). Given the fragility and large size of native MKs, we sought to further substantiate MHC II expression on MKs by visualization *in situ*. Imaging of femoral cryosections confirmed endogenous MHC II expression in a subset of MKs through EGFP and CD41+ co-expression (**Fig 1E**). These findings were corroborated with live cell imaging of native, bone marrow MKs where cell surface MHC II could be observed in a subpopulation of large, polyploid MKs (**Fig 1F**). Notably, we also observed expression of MHC II in splenic megakaryocytes, with an average expression level of 33.37 ± 4.88 (**Fig S1B**), as previously reported (12, 13). These experiments revealed that MHC II is robustly expressed on subpopulations of myeloid progenitors and throughout the MK lineage in the bone marrow, including CD41+ MK biased HSCs, MK progenitors, and mature MKs.

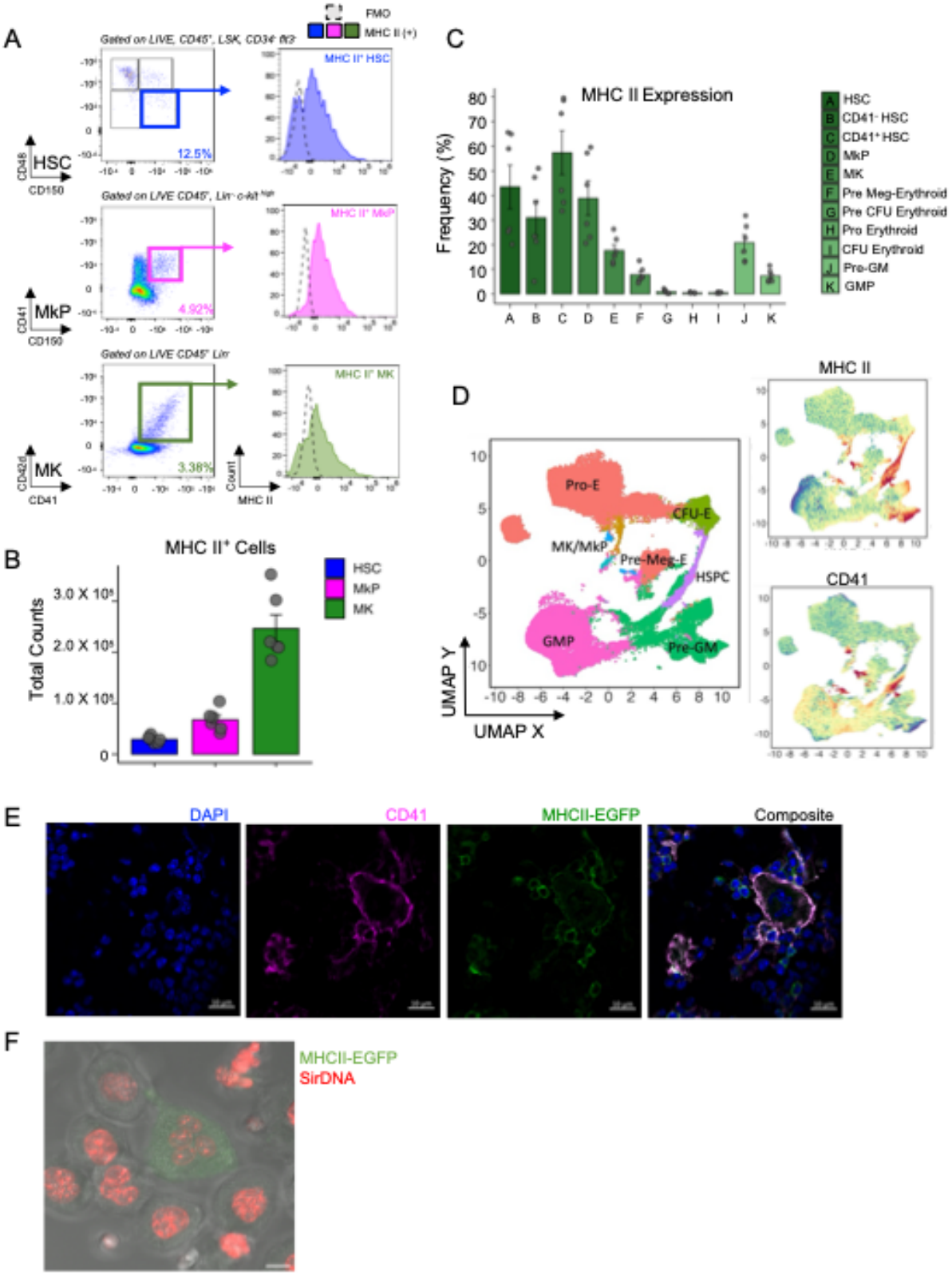
A
FMO
MHC II (+)
Gated on LIVE, CD45+, LSK, CD34- flt3-
MHC II+ HSC
12.5%
HSC
CD48
CD150
Gated on LIVE CD45+, Lin- c-kit hi
MHC II+ MkP
4.92%
MkP
CD41
CD150
Gated on LIVE CD45+ Lin-
MHC II+ MK
3.38%
MK
CD42d
CD41
Count
MHC II
B
MHC II+ Cells
Total Counts
3.0 X 10^5
2.0 X 10^5
1.0 X 10^5
0
HSC
MkP
MK
C
MHC II Expression
Frequency (%)
80
70
60
50
40
30
20
10
0
A B C D E F G H I J K
A HSC
B CD41- HSC
C CD41+ HSC
D MkP
E MK
F Pre Meg-Erythroid
G Pre CFU Erythroid
H Pro Erythroid
I CFU Erythroid
J Pre-GM
K GMP
D
Pro-E
CFU-E
MK/MkP
Pre-Meg-E
HSPC
GMP
Pre-GM
UMAP Y
UMAP X
MHC II
CD41
E
DAPI
CD41
MHCII-EGFP
Composite
F
MHCII-EGFP
SirDNA

FIGURE 1

Fig. 1. MHC II is expressed throughout the megakaryocyte lineage.
(**A**) Representative plots and histogram of MHC II expression in HSCs, MkPs, and MKs.
(**B**) Absolute counts of MHC II^+ cells; *n* = 5 animals.
(**C**) Frequencies of MHC II expression in bone marrow progenitors; *n* = 5 animals.
(**D**) High dimensional flow cytometry UMAP projection of bone marrow progenitors (left); MHC II and CD41 expression (right).
(**E**) Femoral cryosections stained with DAPI, CD41, MHC II; scale bar = 10 µm.
(**F**) Representative images of native megakaryocytes isolated from MHC II-eGFP reporter mice with MHC II+ MKs visualized by endogenous eGFP expression (green) and nuclei stained with SiR-DNA (red); scale bar = 10 µm.
Data are shown as mean ± SD; graphs represent data from at least 3 independent experiments.

MHC II-expressing MKs activate CD4+ T cells ex vivo

We next aimed to determine the functional capacity of MK MHC II. MHC II molecules present peptides to CD4+ T helper cells, which in turn recognize the peptide-MHC II complex via their T-cell receptors (**TCRs**). For robust activation, however, a secondary signal between costimulatory molecules on both the CD4+ T cell and the APC must be provided. As such, we assessed if bone marrow MKs expressed key costimulatory molecules and found that they express CD80/CD86 (B7-1/B7-2), CD40, and CD86 (**Fig 2A**) at baseline, indicating potential APC function. To ascertain if toll-like receptor (**TLR**) activation could influence the expression of the co-stimulatory molecules on MKs, we isolated native bone marrow MKs and treated them ex vivo with Polyinosinic-polycytidylic acid, (**Poly I:C**), a synthetic double-stranded RNA molecule that mimics viral RNA and activates TLR3 and Lipopolysaccharide (**LPS**), which activates TLR4. We observed that LPS led to upregulation of key co-stimulatory molecules on MKs upon stimulation (**Fig 2A**). Given that key costimulatory molecules were upregulated upon TLR stimulation, we next tested the ability of bone marrow MKs to uptake and process antigen. To assess the intracellular degradation (processing) of antigens by bone marrow MKs we utilized DQ-ovalbumin (**OVA-DQ**) in which MKs were treated with BODIPY-conjugated DQ-OVA, a self-quenched conjugate of OVA that exhibits bright green fluorescence only upon proteolytic cleavage releasing the dye molecule from the OVA (**Fig S2A**). After 90 minutes, DQ-OVA fluorescence was observed in MKs, indicating active intracellular proteolytic activity. Thus, we next assayed the ability of MKs to activate naive CD4+ T cells. We used OT-II mice engineered to express a TCR that recognizes specific residues of chicken OVA ($OVA_{323-339}$) presented by MHC II. Bone marrow MKs were isolated, incubated with OVA peptide, and washed to remove unprocessed peptide before culture with naïve CD4+ OT II T cells (**Fig 2B**). We observed peptide-specific activation, as judged by CD25 upregulation, and proliferation of naïve OT-II T cells in conditions where both MKs and OVA were present (**Fig 2B-C**). Correspondingly, addition of an MHC II neutralizing antibody significantly abrogated T cell activation and proliferation (**Fig 2C**, demonstrating that T cell proliferation was an MHC II-dependent interaction. Live cell microscopy further substantiated the direct interactions between MKs and T cells (**Supplementary movie 1)**. Given that T cell differentiation is also regulated by cytokine

secretion, and that MKs are known to secrete TGF-β, we sought to determine how T cell interactions might be influencing this capacity. Indeed, we observed that after 5 days of coculture, MHC II expressing MKs secreted more TGF-β, as quantified by intracellular LAP, in the presence of T cells (**Fig S2B**). As TGF-β is known to drive induced Treg (**iTreg**) differentiation, we characterized the T cell compartment of the cultures. We observed that the presence of MKs increased the frequency of CD25+ Foxp3+ cells and that this was blunted with addition of a TGF-β neutralizing antibody (**Fig S2C**). Together, these results demonstrate that bone marrow MKs can activate naïve T cells in an MHC II-dependent manner, which is complemented by increased TGF-β secretion upon contact with CD4 T cells and iTreg differentiation.

To determine if our observations were applicable to human MKs, we obtained CD34+ cells from femoral head samples of healthy donors and differentiated these into MKs (**Fig 2D**). We then characterized the cell surface expression of HLA-DR in ex vivo generated human MKs. The results mirrored our findings in the murine model; HLA-DR was expressed in approximately 40% of MKs (**Fig 2E**). To determine if antigen-processing capacity was also a feature of human MKs, human MKs were incubated with DQ-OVA. We observed fluorescence resulting from OVA-DQ proteolysis, indicating that human MKs can process antigens, paralleling murine MKs (**Fig 2F**).

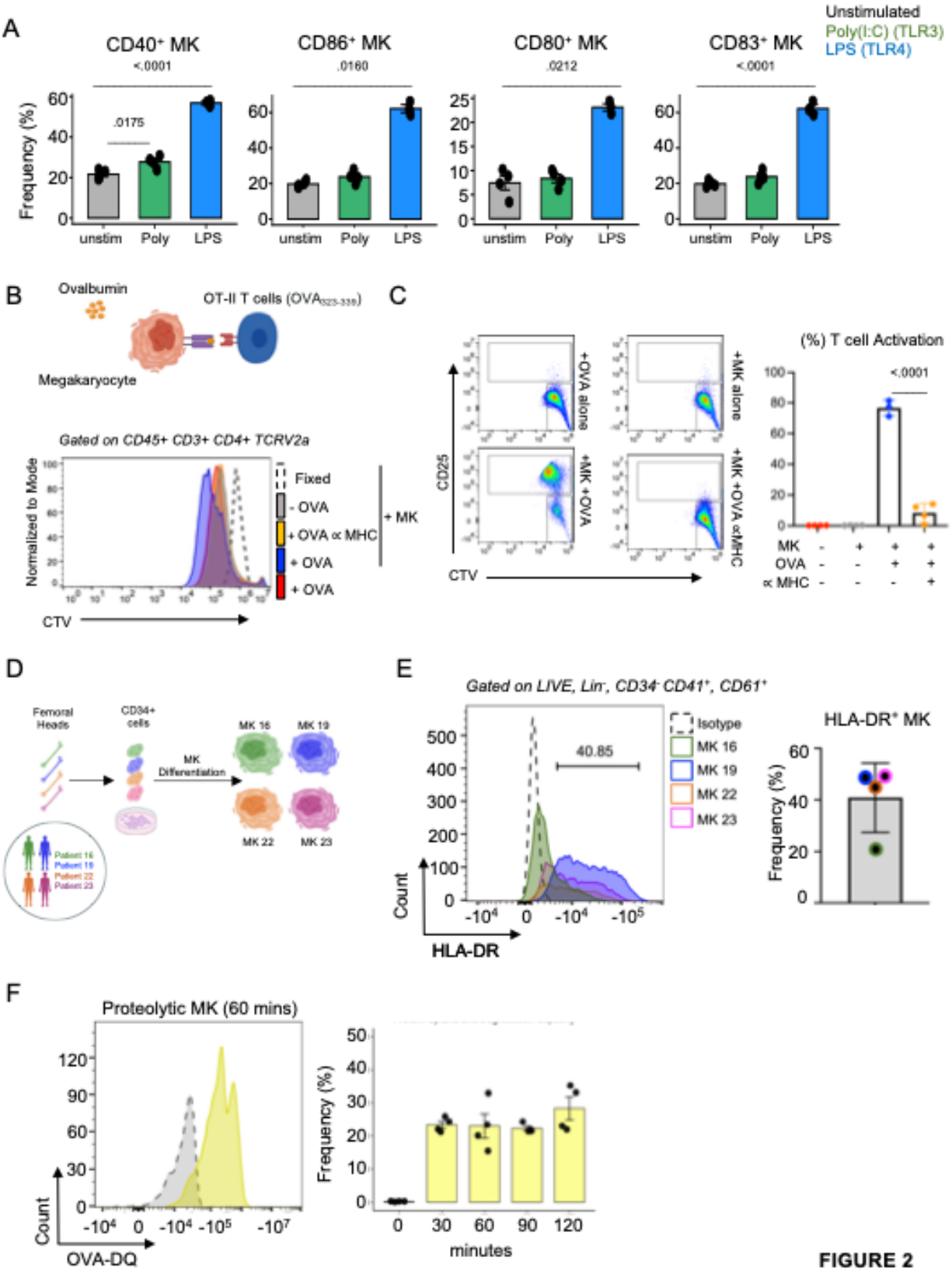
A
Unstimulated
Poly(I:C) (TLR3)
LPS (TLR4)
CD40+ MK
CD86+ MK
CD80+ MK
CD83+ MK
<.0001
.0160
.0212
<.0001
.0175
Frequency (%)
unstim
Poly
LPS
B
Ovalbumin
OT-II T cells (OVA323-339)
Megakaryocyte
Gated on CD45+ CD3+ CD4+ TCRV2a
Normalized to Mode
Fixed
- OVA
+ OVA ∝ MHC
+ OVA
+ OVA
+ MK
CTV
C
+OVA alone
+MK alone
+MK +OVA
+MK +OVA ∝MHC
CD25
CTV
(%) T cell Activation
<.0001
MK
OVA
∝ MHC
D
Femoral Heads
CD34+ cells
MK Differentiation
MK 16
MK 19
MK 22
MK 23
Patient 16
Patient 19
Patient 22
Patient 23
E
Gated on LIVE, Lin-, CD34- CD41+, CD61+
Isotype
MK 16
MK 19
MK 22
MK 23
40.85
Count
HLA-DR
HLA-DR+ MK
Frequency (%)
F
Proteolytic MK (60 mins)
Count
OVA-DQ
Frequency (%)
minutes

FIGURE 2

Fig. 2. MHC II-positive megakaryocytes activate CD4+ T cells ex vivo.
(**A**) Frequencies of CD40, CD86, CD80, and CD83 expressing MKs; *n* = 3 animals.
(**B**) Schematic of MK and naïve CD4+ T cell co-culture (top) and representative histogram of MK and T cell culture conditions in the presence or absence of OVA and anti-MHC antibody.
(**C**) Representative plots of coculture conditions in the presence or absence of OVA and anti-MHC antibody (left); quantification of T cell activation (right). *n* = 4 mice/condition.
(**D**) Schematic of ex vivo MK differentiation from human femoral head samples.
(**E**) Representative histogram of HLA -DR+ human MKs (left) and frequency of expression (right). *n* = 4 donors.
(**F**) Representative histogram of OVA -DQ+ fluorescent MKs (left) and frequency of OVA -DQ+ MKs at 30, 60, 90, and 120 mins (right); *n* = 4 donors.
Data are shown as mean ± SD; graphs represent data from at least 3 independent experiments. Statistics performed with 1-way ANOVA with Tukey's multiple comparisons test at 95% CI (A, C, F).

MHC II is not present on platelets

We next aimed to further characterize MHC+ MKs and determine if MHC II was transferred to platelets. As MKs mature, DNA replication occurs without cytokinesis in a process called endomitosis, leading to polyploidization. In turn, ploidy status correlates with maturation, and higher ploidy in combination with larger cystoplasmic content, correlates with platelet production (22). Analysis of the ploidy status of bone marrow MKs revealed that MHC II expression spread across various ploidy states but predominated in lower ploidy MKs (**Fig 3A-B, S3A**). We and others have previously shown that MKs can transfer MHC I onto platelets, indicating that the machinery to transfer MHC components to platelets is present (23). Therefore, we examined if MHC Class II was present on platelets. First, we analyzed MK and platelet proteomes and compared their protein signature to acellular fractions: bone marrow fluid and peripheral blood plasma (**Fig S3B**). Principal component analysis (PCA) revealed the greatest similarity between the proteomes of bone marrow fluid and MKs, and the greatest difference between the bone marrow fluid, blood plasma, and MKs (**Fig S3C**). To gain insight into proteins transferred from MKs to platelets, we first characterized proteins associated with either class I or class II antigen presentation function across platelets, MKs, blood plasma, and bone marrow fluid (**Fig 3C**). Visualization of antigen presentation proteins revealed proteomic overlap between MKs and platelets. These shared proteins likely represent factors synthesized in MKs and subsequently transferred to platelets during thrombopoiesis. In contrast, proteins detected exclusively in MKs or platelets were considered reflective of cell type–specific biological processes or differential protein turnover. Notably, components of the MHC class I pathway were among the shared proteins, suggesting that MHC class I molecules are transferred from MKs to platelets. Conversely, MHC class II–associated proteins were predominantly confined to MKs, consistent with limited inheritance of class II machinery by platelets (**Fig 3D**). These findings highlight the continuity between MK and platelet proteomes and suggest that platelets do not inherit MHC class II–associated proteins from precursor MKs.

To expand on this, we performed immunostaining of MHC II on resting and activated platelets. We detected no MHC II signal in either condition (**Fig 3E**). To validate this in vivo, we performed two-photon intravital microscopy (2P-IVM) on the calvaria of MHC II–EGFP knock-in mice. To mimic immune activation, mice were treated with LPS, which simulates immune activation via TLR4. However, even upon TLR stimulation, no MHC II was detected in platelets, as assayed by colocalization of GFP and GP1B. (**Fig 3F-G, Supplementary Movies 2-3**). Together, these data suggest that MHC II-expressing MKs are either not platelet-producing, or do not package this molecule into platelets even when MHC II is upregulated.

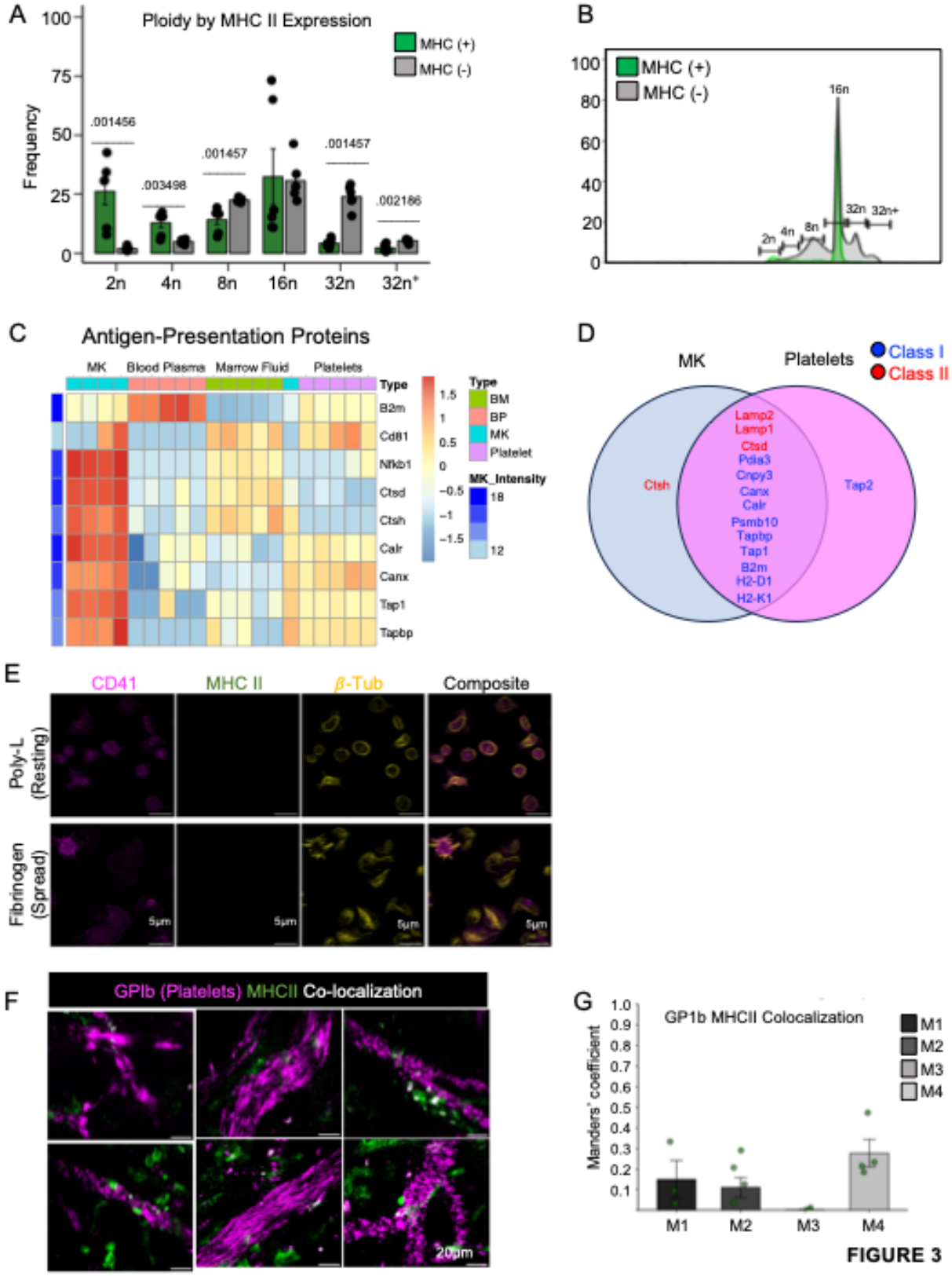
A
Ploidy by MHC II Expression
MHC (+)
MHC (-)
Frequency
.001456
.003498
.001457
.001457
.002186
2n
4n
8n
16n
32n
32n+
B
MHC (+)
MHC (-)
16n
2n
4n
8n
32n
32n+
C
Antigen-Presentation Proteins
MK
Blood Plasma
Marrow Fluid
Platelets
Type
B2m
Cd81
Nfkb1
Ctsd
Ctsh
Calr
Canx
Tap1
Tapbp
BM
BP
MK
Platelet
MK_Intensity
D
MK
Platelets
Class I
Class II
Ctsh
Lamp2
Lamp1
Ctsd
Pdia3
Cnpy3
Canx
Calr
Psmb10
Tapbp
Tap1
B2m
H2-D1
H2-K1
Tap2
E
CD41
MHC II
β-Tub
Composite
Poly-L (Resting)
Fibrinogen (Spread)
5μm
F
GPIb (Platelets) MHCII Co-localization
20μm
G
GP1b MHCII Colocalization
Manders' coefficient
M1
M2
M3
M4

FIGURE 3

Fig. 3. MHC II is present on megakaryocytes but not platelets.
(**A**) Frequencies of DNA ploidy by MHC II expression; *n* = 10 animals.
(**B**) Representative flow plot of MK ploidy distribution by MHC II expression.
(**C**) Heatmap of proteins associated with antigen presentation in MKs, blood plasma, bone marrow fluid, and platelets; *n* = 4 animals.
(**D**) Venn Diagram of MHC I and MHC II proteins shared between MKs and platelets: *n* = 4 animals.
(**E**) Representative images of resting and spread platelets stained for CD41, MHC II, and β1-tubulin; scale bar = 5 µm.
(**F**) Representative two-photon images of calvaria bone marrow from MHC II-eGFP reporter mice (green); platelets visualized by intravenous injection of fluorescently conjugated anti-GPIb antibody (magenta). Areas of colocalization between MHC II+ cells and platelets are shown in white; scale bar = 20 µm.
(**G**) Quantification of platelet and MHC II colocalization. n= 4 mice, with 3–5 fields of view analyzed per mouse.
Data are shown as mean ± SD (A); mean ± SEM (G); graphs represent data from at least 3 independent experiments (A-B, F-G). Data from 1 independent experiment with 4 biological replicates (C-D). Statistics performed with unpaired 2-tailed Student *t* test.

MHC II+ vs MHC II- MKs have differential gene expression

To further define MHC II expressing MKs, we performed bulk RNA sequencing (RNA-seq) of MHC II -positive and -negative MKs. We observed various DE genes between the two subsets while pathway analysis showed an enrichment of functions related to phagocytosis, interferon responses, and cell-adhesion in MHC II-positive MKs. Conversely, MHC II-negative MKs were enriched in functions related to migration, chemotaxis and coagulation (**Fig 4A, S4A-B, Supplementary Table 1**).

To identify the transcriptional regulators driving the differential gene expression between MHC II-positive and MHC II-negative MKs, we employed VIPER analysis in combination with the DoRothEA regulon database. Analysis of the inferred transcription factor (**TF**) activities revealed distinct sets of TFs with elevated activity in each population. In MHC-positive MKs, the top upregulated TFs included Irf4, Rfx5, Irf9, Pparg, and Irf1 (**Fig 4B, S4C**). Predictably, Rfx5 serves as a regulator of MHC class II genes**,** directly driving the expression of antigen presentation machinery; Irfs suggest involvement in immune signaling and antiviral responses, while Pparg indicates involvement in lipid metabolism and potential anti-inflammatory pathways. Overall, this network indicates a strong involvement of interferon regulatory factors and immune-related transcriptional programs.

Conversely, in MHC-negative cells, TFs such as Smad4, Tbx21, Bach1, and Rel exhibited the highest activity, highlighting transcriptional programs potentially involved in TGF-β signaling, oxidative stress response, and NF-κB signaling (**Fig 4B, S4C**). This analysis suggests that different transcription factors likely orchestrate the transcriptional differences between MHC II-

positive and -negative MKs and reveals that the activity of specific interferon-regulated and immune-modulatory TFs is a defining feature of MHC II-positive cells.

Previous work by Sun et al. demonstrated that bone marrow MKs comprise four distinct subsets: platelet-generating MKs, HSC-niche MKs, immune/inflammatory MKs, and actively cycling MKs. These subsets are enriched for unique gene programs and differ in localization within the bone marrow microenvironment. By overlaying our bulk RNA-seq signatures onto their single-cell atlas, we found that both MHC□ and MHC□ MKs mapped to their immune/inflammatory cluster. Intriguingly, MHC□ MKs mapped more closely with the HSC Niche subset while MHC□ MKs were also distributed along the actively cycling MK subset (**Fig 4C**). This distribution suggests that antigen-presenting capacity, as indicated by MHC II expression, is not exclusive to a distinct transcriptionally defined MK subset but rather reflects broader functional plasticity among MK populations.

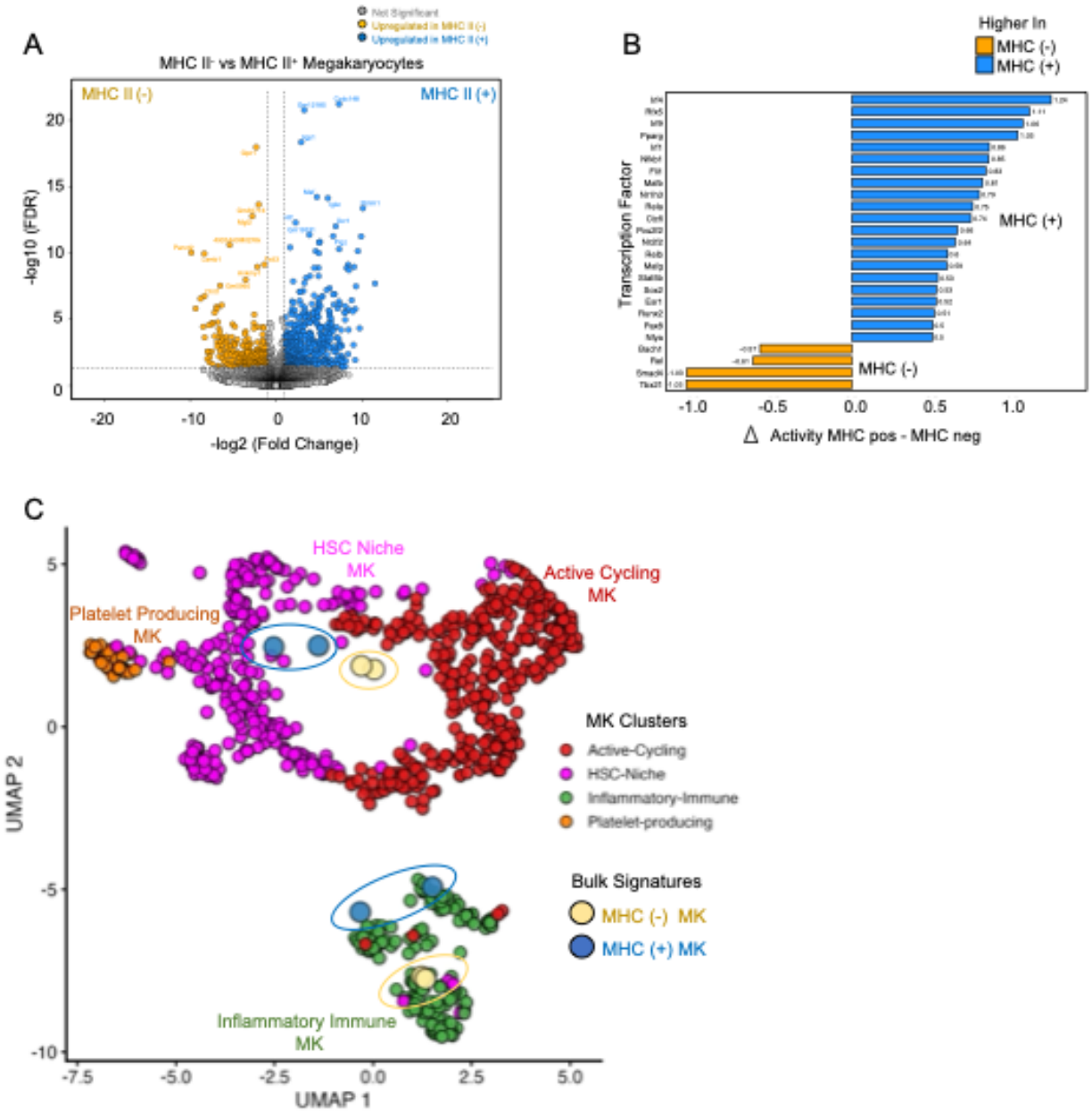
A
MHC II⁻ vs MHC II⁺ Megakaryocytes
MHC II (-)
MHC II (+)
-log10 (FDR)
-log2 (Fold Change)
B
Higher In
MHC (-)
MHC (+)
Transcription Factor
MHC (+)
MHC (-)
Δ Activity MHC pos - MHC neg
C
HSC Niche MK
Active Cycling MK
Platelet Producing MK
Inflammatory Immune MK
UMAP 2
UMAP 1
MK Clusters
Active-Cycling
HSC-Niche
Inflammatory-Immune
Platelet-producing
Bulk Signatures
MHC (-) MK
MHC (+) MK

FIGURE 4

Fig. 4. MHC II-positive megakaryocytes have a unique transcriptome enriched in interferon regulatory factors and immune-related transcriptional programs.
(**A**) Volcano plot of differentially expressed genes between MHC II$^-$ and MHC$^+$ MKs.
(**B**) Bar plot of DE genes integrated with (TF) regulons from the DoRothEA database showing the top 35 TFs ranked by differential activity (Δ activity = MHC□ – MHC□). Bars are colored according to the group in which TF activity was higher (blue, MHC□; orange, MHC□), with values indicating the magnitude of difference in inferred activity.
(**C**) A projection of bulk RNA-seq MHC$^+$ and MHC$^-$ MKS into onto a reference single-cell UMAP embedding of MK subpopulations from Sun et al.

MKs present peptides via MHC II in vivo

To characterize the MHC II-associated peptidome of bone marrow MKs, we performed immunopeptidomics. We employed immuno-capture of MHC II complexes followed by mass spectrometric analysis of eluted peptides, which enabled the identification of MHC II-bound peptides from bone marrow MKs (**Fig 5A**). High-resolution LC-MS/MS of sorted bone marrow MKs identified 290 peptides corresponding to 75 proteins. After filtering for peptide length (≥9 residues), removal of contaminants, and exclusion of MHC-II–derived sequences, the dataset consisted of 78 peptides and 43 parental proteins (**Supplementary Table 2**). Peptide length distribution showed that over 90% were 9–26 amino acids, with a mode of 15 residues, consistent with canonical MHC class II ligands (**Fig S5A**). The GibbsCluster v.2.0 tool was used for unsupervised motif analysis in peptide dataset. The GibbsCluster output for the interest peptide dataset showed a very good agreement with the H2-Ab1 motif described in the database (**Fig S5B**), supportive that the peptides sequenced were isolated from those molecules. To predict the theoretical binding affinity of peptides to murine H2-Ab1 molecules, we utilized the NetMHCIIpan v4.1 tool. By applying 1% rank as a threshold for strong binding (HB) peptides and 5% rank for weak binding (WB) peptides, a 51.3% was assigned as HB and 5.1% as WB (**Fig 5B**). Mapping peptides to their source proteins revealed that a small number of proteins dominated the immunopeptidome. The most abundant was Ferritin light chain 1 (Ftl1), followed by Vimentin (Vim), Adenylyl cyclase-associated protein 1 (Cap1), and Prolow-density lipoprotein receptor–related protein 1 (Lrp1) (**Fig 5C-D**). Nested sets, groups of peptides sharing a common 9-mer binding core but varying in C- and N-terminal lengths, are common among MHC II peptides. We categorized these sequences into clusters which provided a visual approximation of the peptide families present in the dataset. Thirteen clusters were identified, with a notable group being a set of nine peptides derived from the ferritin light chain 1 protein (**Fig 5D**). Classification into protein categories revealed an enrichment of metabolism (52.9%) and cytoskeleton (22.1%) associated proteins (**Fig 5E**). To explore the functional enrichment of the 43 parental proteins from MHC II-isolated peptides, a GO enrichment analysis was performed using annotations from the PANTHER database. The proteins were categorized based on their molecular functions, biological roles, and protein classes. The molecular function analysis highlighted a significant enrichment in binding activities. In terms of biological processes, the main enrichments were in cellular processes and biological regulation (**Fig S5C**).

Lastly, the analysis identified protein-binding activity modulators as the most prevalent protein classes within the group (**Fig S5C**).

MHC-II molecules primarily present peptides derived from exogenous proteins. Proteins are internalized by several pathways, including phagocytosis, macropinocytosis, and endocytosis, and peptides are generated by lysosomal proteolysis (24, 25). Thus, endo-lysosomal degradation pathway includes proteins from cell membrane, extracellular region, Golgi apparatus, endoplasmic reticulum, and endosome/lysosome, while cytosolic pathway of degradation includes cytosolic, mitochondrial, and nuclear proteins. Our results corroborate the MHC II processing of both cytosolic and endo-lysosomal proteins, with 62.8% of parental proteins associated with the endo-lysosomal degradation pathways, and the remainder to cytosolic degradation, suggesting exogenous origin (**Fig S5D**). These findings suggest the receptor is both occupied and functional in vivo and establish a framework for further studies in murine models.

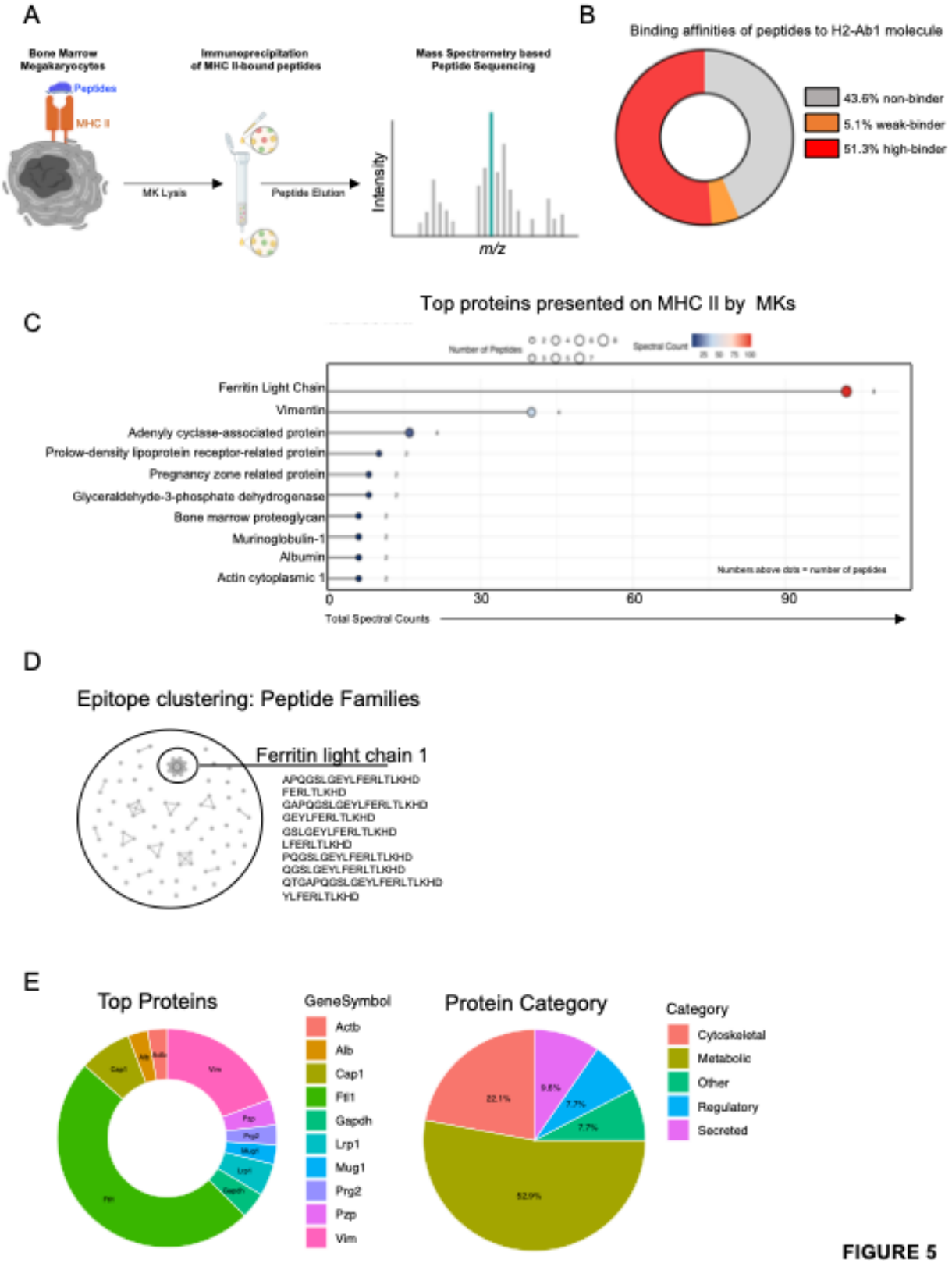
A
Bone Marrow Megakaryocytes
Peptides
MHC II
MK Lysis
Immunoprecipitation of MHC II-bound peptides
Peptide Elution
Mass Spectrometry based Peptide Sequencing
Intensity
m/z
B
Binding affinities of peptides to H2-Ab1 molecule
43.6% non-binder
5.1% weak-binder
51.3% high-binder
C
Top proteins presented on MHC II by MKs
Number of Peptides
Spectral Count
Ferritin Light Chain
Vimentin
Adenyly cyclase-associated protein
Prolow-density lipoprotein receptor-related protein
Pregnancy zone related protein
Glyceraldehyde-3-phosphate dehydrogenase
Bone marrow proteoglycan
Murinoglobulin-1
Albumin
Actin cytoplasmic 1
Numbers above dots = number of peptides
0
30
60
90
Total Spectral Counts
D
Epitope clustering: Peptide Families
Ferritin light chain 1
APQGSLGEYLFERLTLKHD
FERLTLKHD
GAPQGSLGEYLFERLTLKHD
GEYLFERLTLKHD
GSLGEYLFERLTLKHD
LFERLTLKHD
PQGSLGEYLFERLTLKHD
QGSLGEYLFERLTLKHD
QTGAPQGSLGEYLFERLTLKHD
YLFERLTLKHD
E
Top Proteins
GeneSymbol
Actb
Alb
Cap1
Ftl1
Gapdh
Lrp1
Mug1
Prg2
Pzp
Vim
Protein Category
22.1%
9.8%
7.7%
7.7%
52.9%
Category
Cytoskeletal
Metabolic
Other
Regulatory
Secreted

FIGURE 5

Fig. 5. Immunopeptidomics reveals exogenous peptide on MHC II in native bone marrow megakaryocytes.
(**A**) Schematic of bone marrow MK MHC II immunopeptidomics.
(B) Donut plot displaying binding affinities of MK peptides to the H2-Ab1 molecule. The cumulative percentage of high-binder (HB), weak-binder (WB) and non-binder (NB) isolated peptides is shown.
(**C**) Lollipop plot of spectral counts displaying number of peptides in respective protein families.
(**D**) Epitope cluster analysis of MK peptides grouped into clusters based on sequence identity, by applying a threshold of 70%.
(**E**) Donut plot displaying top proteins identified (left) and assigned to protein category (right).

MK-specific loss of MHC II alters stem and progenitor cells following TLR stimulation

To better understand the functional differences between MHC II-expressing and non-expressing MKs and discern the relevance of the MHC II-expressing MKs, we generated a murine model with targeted deletion of MHC II in the MK lineage, *(Pf4-MHC*$^{\Delta/\Delta}$ mice; MHC^{KO} mice). When analyzed by flow cytometry, we observed deletion of MHC II in mature MKs, partial deletion in MkPs and minimal loss of MHC II in HSCs (**Fig S6A**). *Pf4-MHC*$^{\Delta/\Delta}$ mice had no change in MK numbers as quantified by immunofluorescence of femoral cryosections and no change in MK size (**Fig 6A**). As expected, deletion of MHC II on MKs resulted in loss of antigen presentation capacity, and MHC^{KO} MKs were unable to induce naïve T cell activation (**Fig S6B**). Intriguingly, we also observed that in steady state conditions MHC^{KO} MKs had decreased TGF-β1 production as quantified by LAP staining of femoral cryosections (**Fig 6B**) aligning with ex vivo data showing MHC II-expressing MKs produced more TGF-β1 after co-culture of MKs with T cells (**Fig S2C**).

Next, we administered LPS and poly(I:C) to determine if MHC II expression affected MK responses to inflammation. Deletion of MHC II on MKs differentially altered MK expansion and costimulatory molecule expression. Specifically, following LPS administration, MK numbers significantly decreased in *Pf4-MHC*$^{\Delta/\Delta}$ mice. Conversely, MKs expanded in response to poly(I:C) in *Pf4-MHC*$^{\Delta/\Delta}$ mice (**Fig 6C**). Notably, MKs lacking MHC II also had altered expression of costimulatory molecules both at baseline and after stimulation with LPS and poly(I:C) (**Fig 6D**). These findings suggest that MHC II expressing MKs may respond differently to inflammatory cues.

We next examined if deletion of MK MHC II had any effects on stem and progenitor populations, as MKs are also active regulators of the bone marrow niche, and the role of MHC II-expressing MKs on HSPCs is largely unknown. We uncovered a decrease in HSCs and ST-HSCs in *Pf4-MHC*$^{\Delta/\Delta}$ mice but did not detect a change in HSC proliferation (**Fig S6C**). In addition, loss of MHC II in MKs resulted in additional HSPC population alterations in response to TLR stimulation. In *Pf4-MHC*$^{\Delta/\Delta}$ mice treated with LPS, the HSC pool was resistant to depletion, while there was a significant increase in MkP, MPP2, and MPP4 populations. In response to Poly I:C, there was also a slight increase in MPP2 cells **(Fig S6D**). These data

substantiate the in vivo biological relevance of the MHC II receptor on MKs as a modulator of TLR responses and HSC maintenance within the bone marrow.

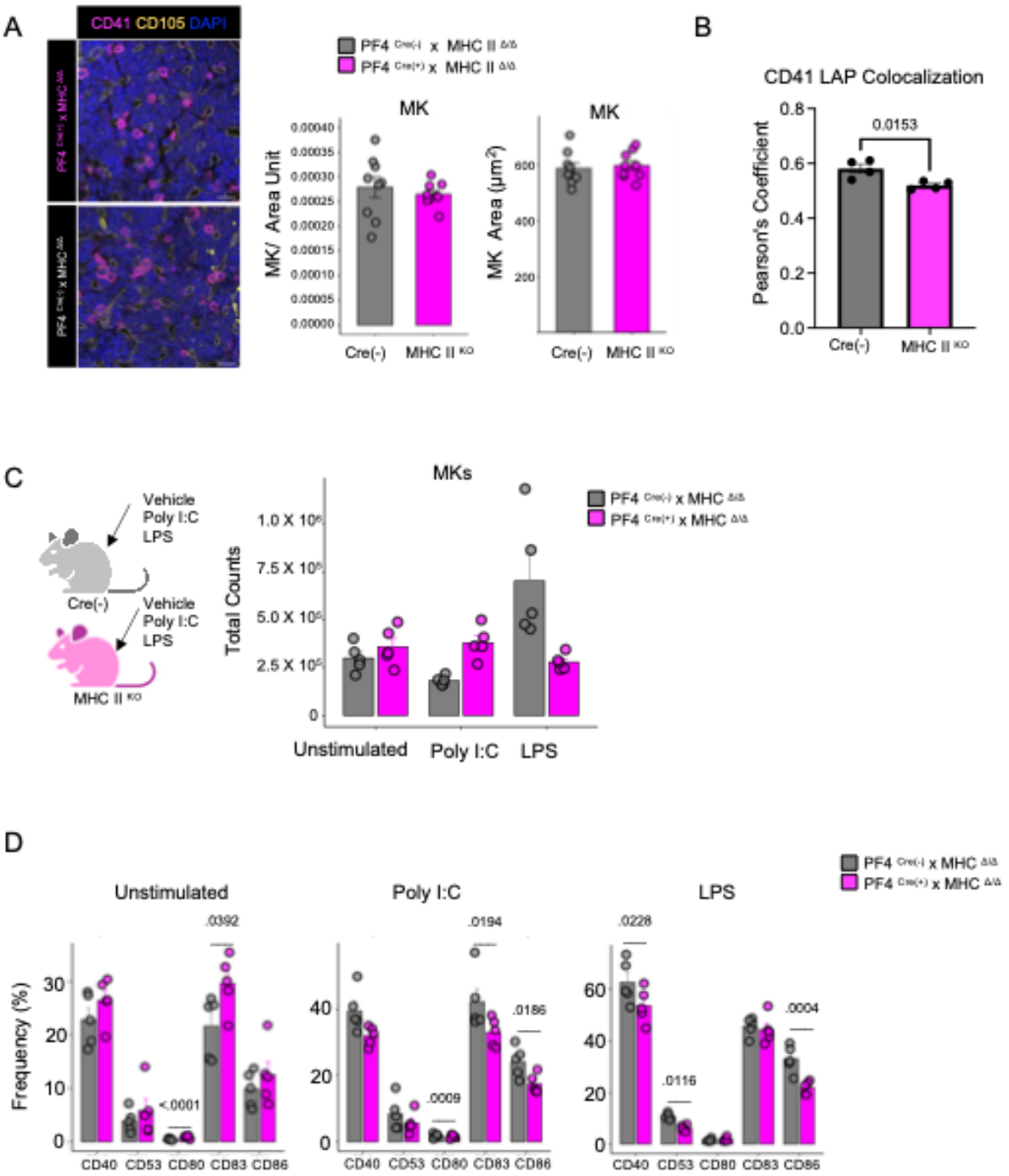
A
CD41 CD105 DAPI
PF4 Cre(-) x MHC II Δ/Δ
PF4 Cre(+) x MHC II Δ/Δ
MK
MK/ Area Unit
MK Area (μm²)
Cre(-)
MHC II KO
B
CD41 LAP Colocalization
Pearson's Coefficient
0.0153
C
Vehicle
Poly I:C
LPS
Cre(-)
MHC II KO
MKs
Total Counts
Unstimulated
Poly I:C
LPS
D
Unstimulated
Poly I:C
LPS
Frequency (%)
CD40
CD53
CD80
CD83
CD86
.0392
<.0001
.0194
.0186
.0009
.0228
.0116
.0004

FIGURE 6

Fig. 6. Megakaryocyte-specific loss of MHC II alters megakaryocyte TLR sensitivity
(**A**) Representative images (left) and quantification of MK numbers and MK area (right) in MHC^{KO} and $Cre^{(-)}$ mice; *n* =10 mice/ genotype.
(**B**) Colocalization analysis of LAP and CD41 on femoral cryosections of MHC^{KO} and $Cre^{(-)}$ mice; *n* =4 mice/ genotype.
(**C**) Total MK counts 24 hours after LPS or Poly (I:C) administration; n= 5 mice/ genotype.
(**D**) Frequency of CD40, CD53, CD80, CD83, CD86 (+) MKs 24 hours after LPS or Poly (I:C) administration; *n* = 5 mice/ genotype. Data are shown as mean ± SD; graphs represent data from at least 3 independent experiments. Statistics performed with unpaired 2-tailed Student *t* test (A–C) and 1-way ANOVA with Tukey' multiple comparisons test at 95.00% CI (C).

DISCUSSION

In this study, we characterized the expression and functionality of MHC II in bone marrow MKs. We demonstrate that a subset of MKs express MHC II and co-stimulatory molecules, are capable of antigen uptake and processing, and can activate naïve CD4 T cells in an MHC II-dependent manner ex vivo. Notably, MHC II was not detected in platelets, even when platelets were activated, indicating that while MKs express MHC II, it is not transferred to platelets. This contrasts with MHC Class I, which is transferred from MKs to platelets and modulates CD8+ T cell responses (23). Using an MHC II–EGFP knock-in mouse and a murine model with targeted deletion of MHC II in the MK lineage, our work expands the understanding of MKs beyond their platelet-producing functions and positions them as immune regulators in the bone marrow.

Our data revealed that bone marrow MKs express not only MHC II but also co-stimulatory molecules such as CD40, CD83, CD80, and CD86. This aligns with transcriptional analyses identifying an "immune MK" subset enriched in antigen presentation and TLR signaling genes (9, 17). Treatment with the TLR agonist LPS enhanced MHC II and co-stimulatory molecule expression on MKs, indicating a functional response. We also established that bone marrow MKs activate CD4+ T cells ex vivo in a peptide-specific manner. Crucially, T cell proliferation was abrogated by MHC II blockade, confirming the dependence. The relevance of these findings extends to human MKs, where similar expression of the MHC II molecule HLA-DR was observed in approximately 40% of human MKs differentiated from healthy donors. Additionally, the capacity for antigen processing was confirmed using a self-quenched DQ-ovalbumin assay, demonstrating that human MKs can internalize and process exogenous antigen. Together, these data establish that MKs possess the hallmarks of APCs and may modulate immune responses in the bone marrow.

To characterize the peptide repertoire presented by MK MHC II under homeostatic conditions, we performed immunopeptidomics. The predominance of Ftl1 and Vim within the MK MHC II immunopeptidome suggests that iron homeostasis and cytoskeletal integrity may be among the cellular processes visible to immune surveillance in the bone marrow. Additional enriched proteins, such as Cap1 and Lrp1, point to potential contributions from vesicular trafficking and lipid metabolism. Overall, these findings indicate that MHC II molecules in MKs capture a

mixture of structural, metabolic, and regulatory proteins. However, the prominence of these peptides could also result from protein abundance or intrinsic peptide–MHC affinity. Moreover, the detection of peptides from these proteins does not establish that the proteins themselves participate in antigen presentation pathways. Further work is necessary to determine how specific peptides influence $CD4^+$ T cell behavior within the marrow niche.

Our data revealed a decrease in HSCs and ST-HSCs in *Pf4-MHC*$^{\Delta/\Delta}$ mice. The bone marrow is increasingly recognized as an immunologically active niche. Our findings, together with recent work by Hass et al. suggest that antigen presentation within the bone marrow is a mechanism for safeguarding hematopoiesis via direct interactions with $CD4^+$ T cells. Our data extend this, suggesting that MHC II MKs can additionally engage $CD4^+$ T cells. Additionally, we found that *Pf4-MHC*$^{\Delta/\Delta}$ mice had a decrease in bone marrow TGF-β, a key cytokine in the induction of Foxp3 Tregs. As such, MHC II-expressing MK-induced TGF-β secretion could contribute to local HSC and immune regulation by inducing the proliferation of Tregs.

We also found that MK-specific deletion of MHC II altered MK responsiveness to TLR agonists. MHC^{KO} MKs had an increased baseline expression of several costimulatory molecules, with the most significant differences in CD80 and CD86. However, upon stimulation with LPS and poly(I:C), MKs lacking MHC II had decreased upregulation of CD80, CD83, and CD86. This reduced induction of costimulatory molecules in MHC II–deficient MKs after TLR stimulation are likely driven by broader, cell-extrinsic changes including the absence of MHC II–dependent feedback from CD4 T cells or shifts in the surrounding immune landscape, both of which normally amplify TLR-driven costimulatory programs.

In summary, our work suggests that bone marrow MKs influence adaptive immunity in the bone marrow. Together with recent findings (18, 26) demonstrating antigen presentation as a safeguard for HSC integrity, our results expand the concept of “immune-active” MKs and hematopoietic cells, suggesting potential avenues for therapeutic targeting in immune-related conditions.

Study Limitations: Our results establish that MKs can activate naive CD4+ T cells to differentiate into Tregs ex vivo via MHC II and TGFβ, and that MK MHC II is peptide-occupied in vivo. However, additional work is necessary to determine if MKs mediate antigen-specific CD4+ T cell priming in vivo. Moreover, while our proteomic analysis and imaging did not detect MHC II on platelets, these approaches may not exclude extremely rare or transient expression on newly released platelet subsets and/or in specific disease conditions. In our immunopeptidomics analysis, peptide length distribution showed that over 90% were 9–26 amino acids, with a mode of 15 residues (**Fig S5A**), and motif analysis agreed with H2-Ab1 (**Fig S5B**), supporting bona fide class II ligands. While GO-based endo-lysosomal annotations (**Fig S5D**) align with exogenous processing routes, these compartments also handle endogenous membrane and organelle turnover; thus, source attribution remains inferential without in vivo tracers. There are also key limitations to our *Pf4-MHC*$^{\Delta/\Delta}$ mouse model. Given the minimal HSC deletion observed (**Fig S6A**) and the expression of *PF4* in the HSC compartment we cannot fully exclude direct

HSC-intrinsic contributions to HSPC phenotypes and TLR responses in *Pf4-MHC*$^{\Delta/\Delta}$ mice or the fact that deletion in a small number of HSC results in partial deletion across all other differentiated lineages stemming from this pool (27).

MATERIALS AND METHODS

Study design

This study was designed to investigate the function and phenotype of MHC II expressing megakaryocytes (MKs) in the bone marrow. Methods include immunopeptidomics, bulk RNA-seq, flow cytometry, immunofluorescent microscopy, confocal imaging, live cell imaging, and ex vivo culture systems. Details of biological replicates, experimental replicates, and statistical analyses are provided in the corresponding figure legends. All details of experimental parameters are provided in Materials and Methods or the Supplementary Materials sections. For image analyses, the study design was blinded to investigators.

Murine strains

C57BL6 mice (stock no. 000664), OT-II mice (stock no. 004194), Pf4-Cre mice (stock no. 008535), *MHCII* $^{fl/fl}$ mice (stock no. 037709), and Foxp3^{EGFP} mice (stock no 006772) were obtained from The Jackson Laboratory. *I-A*^{b}β-eGFP mice were described previously and were bred in the Harvard Medical School animal facility (21).

Immunopeptidomics: Megakaryocyte sort and lysis

Bone marrow MKs were sorted (Live Lineage^{-} CD45^{+} SYTO-40^{+}, CD41^{+}CD42d^{+}) from 10 to 12-week-old B6 mice into PBS. Pellets were snap frozen. Samples were pooled and lysed/solubilized as follows: 500 µL of 50 mM Tris-HCl, 150 mM NaCl (pH 8.0), 1x complete protease inhibitor cocktail, and 1% n-Dodecyl-β-D-maltoside (DDM) were added to sample 1, and 500 µL of 50 mM Tris-HCl, 150 mM NaCl (pH 8.0), 1x complete protease inhibitor cocktail, and 1% NP-40 were added to sample 2. Four cycles of 5-second sonication/5-second break were carried out on ice. Samples were incubated for 30 min in rotation at 4 ºC, followed by centrifugation at 20,000 x g for 1 h at 4ºC. Supernatants were collected and one aliquot was taken for western blot (WB) analysis (2%), and one for protein quantification by BCA. WB conditions were as follows: Primary antibody; Hamster/mouse anti-mouse MHC Class II (βchain), clone KL277 (1/500; o/n incubation) and Secondary antibody; Fluorescent goat anti-mouse IgG (1/10,000; 1h incubation).

Immunopeptidomics: Immunoprecipitation (IP)

The supernatant containing solubilized membranes (SB) was incubated overnight (o/n) at 4 °C, with an anti-mouse MHC Class II (I-A/I-E) antibody (Ab), clone M5/114, coupled to CNBr-activated sepharose beads: 20 µL of a 0.5x preparation of Ab-beads coupled at 2 mg Ab per 1 mL of hydrated beads were added. After o/n incubation, sample was loaded into a Bio-Spin Chromatography Column (Bio-Rad). Non-retained (NR) fraction was collected and sequential washes were performed on the retained fraction: 3x 50 mM Tris-HCl, 150 mM NaCl (pH 8.0), 0.5% DDM; 3x 50mM Tris-HCl, 150 mM NaCl (pH 8.0); 1x 50 mM Tris-HCl, 0.5M NaCl (pH 8.0); 3x 50 mM Tris-HCl, 150 mM NaCl (pH 8.0); and 2x 20 mM Tris-HCl (pH 8.0). Peptides

were eluted with 0.25% trifluoroacetic acid (TFA) and stored at -80 ºC. Aliquots of 5% NR and 10% of eluates (EL) were collected for WB analysis to assess the yield of IP.

Immunopeptidomics: Mass spectrometry (MS) analysis

Sample was evaporated to dryness, reconstituted in 2.5% TFA, and loaded into ZiptipsC18 pipette tips for desalting. Sample was then fractionated by strong cation-exchange chromatography using GELoader epTIPS loaded in house with polysulfoethyl-A. Elution with NH_4Cl at 25 and 75 mM in 30% acetonitrile (ACN) / 0.1% formic acid (FA) was applied. The fractions were evaporated to dryness and reconstituted in 5% methanol / 0.5% TFA for MS analysis. The MS system used was a 480 Exploris mass spectrometer (ThermoFisher) coupled to ACQUITY UPLC M-Class chromatographic system (Waters). The separation was conducted at 500 nL/min, gradient 0-30% ACN (0.1% FA) in 60 min. The spectrometric analysis was performed in a data dependent mode, HCD fragmentation, Top speed method. The range acquired was 400-1,600 m/z. LC-MS/MS spectra were searched using SEQUEST (Proteome Discoverer v3.0, ThermoFisher) with the following parameters: peptide mass tolerance 10 ppm, fragment tolerance 0.02 Da, and dynamic modification of methionine oxidation (+15.995 Da). The database used for searching was created by combination of *Mus musculus* (Uniprot), and common proteomics contaminants database (MaxQuant). After filtering results by high peptide confidence (1% FDR), 290 peptides and 75 proteins were obtained from database search.

Proliferation Assay via EdU

A total of 1 mg/mouse of EdU in 200 μL PBS was administered intraperitoneally (i.p.) 16 hours before being euthanized for analysis. Cells were analyzed 16 hours after injection, and EdU incorporation was assessed according to the manufacturer's protocol.

Flow cytometry and cell sorting

Cell surface staining was performed following Fc blocking (TruStain FcX™, anti-mouse CD16/32) by incubating single cell suspensions. Cells were then stained with surface markers. A viability dye (Life Technologies, Aqua, dilution 1:1000) was applied to exclude dead cells and SYTO™ 40 Blue (S1135, ThermoFisher Scientific) was used to indicate viable cells. MKs were sorted using a 130 um nozzle and BD FACSymphony™ S6 Cell Sorter. For immunophenotyping, data was acquired and unmixed using SpectroFlo® v2.2.0.3 software (Cytek Biosciences, Fremont, California, USA). FlowJo (Tree Star Inc.) was used for data analysis. High-dimensional analysis was conducted using *Spectre* toolkit in R (v.4.5.1).

Megakaryocyte isolation by size exclusion

Bone marrow cells from femora, tibiae, and iliac crests were isolated by centrifugation for 40 seconds at 2000 x g and primary MKs were isolated as described (28). Briefly, red blood cells were lysed for 5 mins in ACK buffer (A1049201, Gibco) and cells were passed through a 100

µm cell strainer. The cell suspension was consecutively filtered using 20 and 15 µm cell strainers (43-50020-03 and 43- 50015-03, pluriSelect) and MKs were retrieved by inverting strainers.

Naïve CD4 T cell isolation

Naïve CD4 T cells were isolated from mouse spleen single-cell suspensions using the EasySep™ Mouse Naïve CD4 T Cell Isolation Kit (STEMCELL Technologies, Cat. #19765), according to the manufacturer's protocol.

Murine ex vivo cultures

Naïve CD4+ T cells were isolated and labelled with cell trace violet (ThermoFisher) according to manufacturer's instructions. $4x10^4$ naïve CD4+ T cells were cultured with $1x10^4$ MKs and Ovalbumin peptides (OVA-323-339, 25mg/mL, InvivoGen) for 4-5 days. Cells were cultured at 37°C and 5% CO_2 in U-bottom plates in a total volume of 200 mL of Dulbecco's Modified Eagle's Medium, GlutaMAX (DMEM GlutaMAX, Gibco) supplemented with 50 ng mL^{-1} TPO, 10% heat-inactivated Fetal Bovine Serum (FBS), sodium pyruvate, (1.5mM, Gibco), L-glutamine (2mM, Gibco), L-arginine (1x, Sigma), L-asparagine (1x, Sigma), penicillin/streptomycin (100 U/mL,Sigma), MEM non-essential amino acids (1x, ThermoFisher), and β-mercaptoethanol (57.2 mM, Sigma). As indicated, αMHC-II blocking antibody (10 mg/mL, M5/114.15.2, BioXCell) or a control IgG2b antibody (10 mg/mL, eB149/10H5, ThermoFisher) were added to cultures.

Ex Vivo iTreg cell induction

Sorted naïve $CD4^+CD62L^+$*Foxp3*$^{EGFP-}$ T cells (4×10^4) were stimulated with Dynabeads® Mouse T-Activator CD3/CD28 (11452D, Fisher Scientific) at a bead-to-cell ratio of 2:1 in the presence or absence of 1×10^4 MKs. As indicated, anti-TGF-β (1,2,3) (10 µg/mL, MAB1835, R&D Systems) was added to the cultures.

Murine megakaryocyte differentiation

MKs were differentiated from murine lineage depleted cells harvested from femurs and tibias of 8–12-week-old B6 mice. Progenitor cells from the bone marrow cell suspension were enriched by depleting mature, lineage$^+$ cells expressing CD3ε (clone 145-2C11), CD19 (clone 1D3), B220 (clone RA3-6B2), NK1.1 (clone PK136), CD11b (clone M1/70), CD11c (clone N418), Ly6G/C (clone RB6-8C5), and/or Ter119 (clone TER-119) followed by magnetic bead isolation using DynabeadsTM (11415D, ThermoScientific). Enriched progenitor cells were supplemented with 50 ng mL^{-1} TPO (DMEM, 10% FBS, 2 mM glutamine, 100 IU/mL penicillin/streptomycin,). Cells were cultured in a 37 °C, 5% CO_2 environment for 8 days, after which mature MKs were enriched using size exclusion as described.

Human megakaryocyte differentiation

CD34+ hematopoietic progenitor cells were isolated using the *EasySep*™ Human CD34 Positive Selection Kit (STEMCELL Technologies, Cat. #100-1568), according to the manufacturer's

protocol. Cells were cultured in StemSpan medium (STEMCELL Technologies) supplemented with penicillin/streptomycin (100 U/mL,Sigma), L-glutamine (2 mM, Gibco),10 ng/mL TPO and 10 ng/mL interleukin-11 (Peprotech, UK) for 13 days.

Cryosectioning and immunofluorescence staining

Tissues were fixed in 4% paraformaldehyde (PFA) in PBS overnight at 4°C, then sequentially cryoprotected in 10%, 20%, and 30% sucrose solutions prepared in PBS (each for 24 hours at 4°C). Dehydrated femurs were embedded in a water-soluble embedding medium and frozen at −20 °C. Using a tape transfer system (Kawamoto)(29), 10 µm cryosections were collected with a cryostat (Leica Biosystems). Sections were rehydrated in PBS for 20 min, blocked with 10% donkey serum and subsequently stained. Femoral cryosections were stained with CD105 (AF1320, R&D Systems), laminin (L9393, Sigma-Aldrich), LAP (AF-246-NA, R&D Systems), CD41 (133902, BioLegend) or CD42b (M-051-0, Emfret Analytics). Nuclei were stained using 4′,6-diamidino-2-phenylindole (DAPI). After washing in PBS with 0.1% Triton X-100, slides were mounted using Fluoroshield (F6182, Sigma-Aldrich) and imaged on a Zeiss LSM880 confocal microscope (20× objective). Whole femora were imaged on either a Lionheart automated microscope (BioTek) with a 4× objective, and MKs were quantified using Gen5 software. Mean fluorescent intensities (MFIs) were calculated and colocalization analysis was performed with Fiji Software (Version 2.14.0, NIH).

Immunofluorescence staining of megakaryocytes and platelets

Primary bone marrow-derived or cultured MKs were isolated as described above and fixed in 4% PFA/PBS containing 0.1% Tween20 for 20 min at RT. Cells were spun down at 300 x g for 5 min and nonspecific antibody binding was blocked using 3% BSA/PBS. MKs were plated in 8-well chambers (155360, Nunc Lab-Tek), coated with an anti-mouse-CD31 antibody (102502, BioLegend) for 24h and fixed with 4% paraformaldehyde. MKs and platelets were stained overnight using antibodies against LAP (AF246-NA, R&D Systems), a-tubulin (322588, ThermoFisher Scientific), proplatelet basic protein (PPBP), (PA5-47947, Invitrogen), CD42a (M-051-0, Emfret Analytics), Ovalbumin, Alexa Fluor™ 647 Conjugate (Thermo Fisher Scientific), nuclei were stained using DAPI. Cells were imaged at a Zeiss LSM880 confocal microscope (40x or 63x oil objective)

Megakaryocyte ploidy by flow cytometry

Bone marrow single-cell suspensions were generated, and surface antigens' staining was performed for 30 min on ice. Cells were then fixed, stained for SYTO™ 40 Blue (S1135, ThermoFisher Scientific) and analyzed according to the manufacturers protocol for True-Nuclear™ Transcription Factor Buffer Set (424401, Biolegend). MK DNA content was assessed by quantifying SYTO-40 distribution by flow cytometry.

Live Cell Imaging of native megakaryocytes

Native MKs were isolated from the bone marrow of MHC II-eGFP mice as described. Cells were stained with SiR-DNA (1 μM, Cytoskeleton Inc.) for nuclear visualization and imaged live using a confocal fluorescence microscope (objective 63×, oil immersion). Brightfield and fluorescence channels were acquired simultaneously, and representative images were processed using ImageJ for background subtraction and contrast enhancement.

Two-Photon intravital imaging of the calvaria

Intravital imaging of the bone marrow calvaria was performed as described (1). Briefly, a cranial window was generated by carefully thinning the parietal bone of anesthetized MHC II-EGFP reporter mice to allow optical access to the calvaria bone marrow. Mice were maintained under isoflurane anesthesia throughout the procedure, and body temperature was kept constant using a feedback-controlled heating pad. To visualize circulating platelets, mice received an intravenous injection of fluorescently conjugated anti-GPIbα antibody (0.1 μg/g body weight) immediately prior to imaging. Imaging was performed using a two-photon laser scanning microscope (excitation 920 nm, 20× water immersion objective). Image acquisition parameters (laser power, detector gain, and frame rate) were kept constant between experimental groups.

For image analysis, 3D reconstructions were generated using Imaris (Bitplane), and colocalization between MHC II-EGFP+ cells and platelets was quantified using the Manders overlap coefficient on background-subtracted and thresholded images. Data were averaged from at least three independent fields per mouse, and four mice were analyzed.

RNA Isolation

MKs (Live Lineage^{-} CD45^{+} SYTO-40^{+}, CD41^{+}CD42d^{+}) were sorted from 10 to 12-week-old B6 mice and resuspended in Buffer RLT. RNA was extracted using RNeasy micro kit (QIAGEN), with 4 biological replicates per group.

Bulk RNA Sequencing Analysis

Raw paired-end FASTQ files were processed using a standardized RNA-seq pipeline. Read quality was assessed with FastQC before and after trimming. Adapter removal and quality filtering were performed using fastp with default parameters. The GENCODE mouse reference (vM35, GRCm39) was downloaded and used to build a genome index with RSEM, enabling alignment through STAR. Gene-level quantification was performed with rsem-calculate-expression using the options --star, --paired-end, and --strandedness reverse. Gene counts matrices were generated by combining the RSEM outputs across samples and filtering out genes with fewer than 10 total counts. Differential expression analysis between MHC-positive and MHC-negative groups was carried out using DESeq2 in R. Log2 fold changes were shrunk using ashr method, and genes with |log2 fold change| > 1 and adjusted p-value < 0.05 were considered differentially expressed. Functional enrichment analysis of up- and down-regulated genes was

performed using clusterProfiler and msigdbr against the MSigDB C5 (Gene Ontology Biological Process) category.

Integration of single cell dataset with bulk sequencing

Normalized bulk RNA-seq profiles were projected onto a reference single-cell UMAP embedding to enable comparative visualization across modalities. Gene-level expected counts from RSEM quantification were imported into R, filtered for low-expression genes (row sums >10), and variance-stabilized using the vst() function from DESeq2. The resulting log2-transformed matrix was harmonized with the single-cell dataset (Seurat object) by matching Ensembl or gene symbol identifiers. Shared highly variable genes (HVGs) were used to compute Pearson correlations between bulk and single-cell profiles (bulk × cell matrix). Correlation vectors were transformed into 2D coordinates through a k-nearest neighbors (k=100) weighted averaging of the UMAP positions of the most correlated single cells. The resulting projected coordinates were visualized as blue or yellow markers circles on the single-cell UMAP using ggplot2 and ggrepel.

Transcription Factor Activity Inference

Transcription factor (TF) activity was inferred using the VIPER algorithm implemented via the decoupleR package with regulons obtained from DoRothEA (mus musculus version). Regulons with confidence levels A–C were included. Variance-stabilized expression values served as input, and activity scores were calculated for each TF in each sample. Mean activity per TF per group was calculated and differential activity (Δ Activity) was defined as the difference between MHC-positive and MHC-negative mean scores. TFs were ranked by the absolute magnitude of Δ Activity, and the top TFs (n = 35) were selected for visualization.

Statistics

Statistical analyses are reported as mean ± SD or ± SEM. A Shapiro-Wilk test was used to determine normal versus abnormal distributions, and all continuous variables were tested for mean differences. Depending on the spread of variable, both nonparametric Mann-Whitney *U* test, ANOVA, Kruskal-Wallis, and Wilcoxon tests and parametric 2-tailed Student's *t* test and 1- or 2-way ANOVA were used. For ANOVA, Tukey's post hoc test was used to compare individual groups. Data were analyzed and visualized using R (v.4.5.1).

Supplementary Materials

Supplementary Figures S1 to S6
Supplementary Tables 1-2
Supplementary Movies 1, 2, and 3

References and Notes

1. Asquith NL, Carminita E, Camacho V, Rodriguez-Romera A, Stegner D, Freire D, Becker IC, Machlus KR, Khan AO, Italiano JE. The bone marrow is the primary site of thrombopoiesis. Blood. 2024 Jan 18;143(3):272-278. eng. Conflict-of-interest disclosure: J.E.I. has financial interest in and is a founder of StellularBio, a biotechnology company focused on making donor-independent platelet-like cells at scale; these interests are managed by Boston Children's Hospital. The remaining authors declare no competing financial interests. doi:10.1182/blood.2023020895. Cited in: Pubmed; PMID 37879046.

2. Bruns I, Lucas D, Pinho S, Ahmed J, Lambert MP, Kunisaki Y, Scheiermann C, Schiff L, Poncz M, Bergman A, Frenette PS. Megakaryocytes regulate hematopoietic stem cell quiescence through CXCL4 secretion. Nat Med. 2014 Nov;20(11):1315-20. eng. Epub 20141019. doi:10.1038/nm.3707. Cited in: Pubmed; PMID 25326802.

3. Zhao M, Perry JM, Marshall H, Venkatraman A, Qian P, He XC, Ahamed J, Li L. Megakaryocytes maintain homeostatic quiescence and promote post-injury regeneration of hematopoietic stem cells. Nat Med. 2014 Nov;20(11):1321-6. eng. Epub 20141019. doi:10.1038/nm.3706. Cited in: Pubmed; PMID 25326798.

4. Olson TS, Caselli A, Otsuru S, Hofmann TJ, Williams R, Paolucci P, Dominici M, Horwitz EM. Megakaryocytes promote murine osteoblastic HSC niche expansion and stem cell engraftment after radioablative conditioning. Blood. 2013 Jun 27;121(26):5238-49. eng. Epub 20130510. doi:10.1182/blood-2012-10-463414. Cited in: Pubmed; PMID 23667055.

5. Dominici M, Rasini V, Bussolari R, Chen X, Hofmann TJ, Spano C, Bernabei D, Veronesi E, Bertoni F, Paolucci P, Conte P, Horwitz EM. Restoration and reversible expansion of the osteoblastic hematopoietic stem cell niche after marrow radioablation. Blood. 2009 Sep 10;114(11):2333-43. eng. Epub 20090511. doi:10.1182/blood-2008-10-183459. Cited in: Pubmed; PMID 19433859.

6. Zhao M, Ross JT, Itkin T, Perry JM, Venkatraman A, Haug JS, Hembree MJ, Deng CX, Lapidot T, He XC, Li L. FGF signaling facilitates postinjury recovery of mouse hematopoietic system. Blood. 2012 Aug 30;120(9):1831-42. eng. Epub 20120716. doi:10.1182/blood-2011-11-393991. Cited in: Pubmed; PMID 22802336.

7. Heazlewood SY, Neaves RJ, Williams B, Haylock DN, Adams TE, Nilsson SK. Megakaryocytes co-localise with hemopoietic stem cells and release cytokines that up-regulate stem cell proliferation. Stem Cell Res. 2013 Sep;11(2):782-92. eng. Epub 20130528. doi:10.1016/j.scr.2013.05.007. Cited in: Pubmed; PMID 23792434.

8. Pinho S, Marchand T, Yang E, Wei Q, Nerlov C, Frenette PS. Lineage-Biased Hematopoietic Stem Cells Are Regulated by Distinct Niches. Dev Cell. 2018 Mar 12;44(5):634-641.e4. eng. Epub 20180215. doi:10.1016/j.devcel.2018.01.016. Cited in: Pubmed; PMID 29456137.

9. Sun S, Jin C, Si J, Lei Y, Chen K, Cui Y, Liu Z, Liu J, Zhao M, Zhang X, Tang F, Rondina MT, Li Y, Wang QF. Single-cell analysis of ploidy and the transcriptome reveals functional and spatial

divergency in murine megakaryopoiesis. Blood. 2021 Oct 7;138(14):1211-1224. eng. doi:10.1182/blood.2021010697. Cited in: Pubmed; PMID 34115843.

10. Psaila B, Wang G, Rodriguez-Meira A, Li R, Heuston EF, Murphy L, Yee D, Hitchcock IS, Sousos N, O'Sullivan J, Anderson S, Senis YA, Weinberg OK, Calicchio ML, Iskander D, Royston D, Milojkovic D, Roberts I, Bodine DM, Thongjuea S, Mead AJ. Single-Cell Analyses Reveal Megakaryocyte-Biased Hematopoiesis in Myelofibrosis and Identify Mutant Clone-Specific Targets. Mol Cell. 2020 May 7;78(3):477-492.e8. eng. Declaration of Interests The authors declare no relevant competing interests. doi:10.1016/j.molcel.2020.04.008. Cited in: Pubmed; PMID 32386542.

11. Wang H, He J, Xu C, Chen X, Yang H, Shi S, Liu C, Zeng Y, Wu D, Bai Z, Wang M, Wen Y, Su P, Xia M, Huang B, Ma C, Bian L, Lan Y, Cheng T, Shi L, Liu B, Zhou J. Decoding Human Megakaryocyte Development. Cell Stem Cell. 2021 Mar 4;28(3):535-549.e8. eng. Declaration of Interests The authors declare no competing interests. Epub 20201218. doi:10.1016/j.stem.2020.11.006. Cited in: Pubmed; PMID 33340451.

12. Livada AC, McGrath KE, Malloy MW, Li C, Ture SK, Kingsley PD, Koniski AD, Vit LA, Nolan KE, Mickelsen D, Monette GE, Maurya P, Palis J, Morrell CN. Long-lived lung megakaryocytes contribute to platelet recovery in thrombocytopenia models. J Clin Invest. 2024 Sep 19;134(22). eng. Conflict of interest: The authors have declared that no conflict of interest exists. Epub 20240919. doi:10.1172/jci181111. Cited in: Pubmed; PMID 39302653.

13. Pariser DN, Hilt ZT, Ture SK, Blick-Nitko SK, Looney MR, Cleary SJ, Roman-Pagan E, Saunders J, 2nd, Georas SN, Veazey J, Madere F, Santos LT, Arne A, Huynh NP, Livada AC, Guerrero-Martin SM, Lyons C, Metcalf-Pate KA, McGrath KE, Palis J, Morrell CN. Lung megakaryocytes are immune modulatory cells. J Clin Invest. 2021 Jan 4;131(1). eng. Conflict of interest: The authors have declared that no conflict of interest exists. doi:10.1172/jci137377. Cited in: Pubmed; PMID 33079726.

14. Vono M, Lin A, Norrby-Teglund A, Koup RA, Liang F, Loré K. Neutrophils acquire the capacity for antigen presentation to memory CD4(+) T cells in vitro and ex vivo. Blood. 2017 Apr 6;129(14):1991-2001. eng. Epub 20170131. doi:10.1182/blood-2016-10-744441. Cited in: Pubmed; PMID 28143882.

15. Jin H, Aziz M, Murao A, Kobritz M, Shih AJ, Adelson RP, Brenner M, Wang P. Antigen-presenting aged neutrophils induce CD4+ T cells to exacerbate inflammation in sepsis. J Clin Invest. 2023 Jul 17;133(14). eng. Conflict of interest: The authors have declared that no conflict of interest exists. Epub 20230717. doi:10.1172/jci164585. Cited in: Pubmed; PMID 37463445.

16. Rostami J, Fotaki G, Sirois J, Mzezewa R, Bergström J, Essand M, Healy L, Erlandsson A. Astrocytes have the capacity to act as antigen-presenting cells in the Parkinson's disease brain. J Neuroinflammation. 2020 Apr 16;17(1):119. eng. The authors declare that they have no competing interests. Epub 20200416. doi:10.1186/s12974-020-01776-7. Cited in: Pubmed; PMID 32299492.

17. Hernández-Malmierca P, Vonficht D, Schnell A, Uckelmann HJ, Bollhagen A, Mahmoud MAA, Landua SL, van der Salm E, Trautmann CL, Raffel S, Grünschläger F, Lutz R, Ghosh M, Renders S, Correia N, Donato E, Dixon KO, Hirche C, Andresen C, Robens C, Werner PS, Boch T, Eisel D, Osen W, Pilz F, Przybylla A, Klein C, Buchholz F, Milsom MD, Essers MAG, Eichmüller SB, Hofmann WK, Nowak D, Hübschmann D, Hundemer M, Thiede C, Bullinger L, Müller-Tidow C, Armstrong SA, Trumpp A, Kuchroo VK, Haas S. Antigen presentation safeguards the integrity of the hematopoietic stem cell pool. Cell Stem Cell. 2022 May 5;29(5):760-775.e10. eng. Declaration of interests V.K.K. is a cofounder, has ownership interest, and is on the SAB of Celsius Therapeutics and Tizona Therapeutics. doi:10.1016/j.stem.2022.04.007. Cited in: Pubmed; PMID 35523139.

18. Liao W, Liu C, Yang K, Chen J, Wu Y, Zhang S, Yu K, Wang L, Ran L, Chen M, Chen F, Xu Y, Wang S, Wang F, Zhang Q, Zhao J, Ye L, Du C, Wang J. Aged hematopoietic stem cells entrap regulatory T cells to create a prosurvival microenvironment. Cell Mol Immunol. 2023 Oct;20(10):1216-1231. eng. The authors declare no competing interests. Epub 20230830. doi:10.1038/s41423-023-01072-3. Cited in: Pubmed; PMID 37644165.

19. Hirata Y, Furuhashi K, Ishii H, Li HW, Pinho S, Ding L, Robson SC, Frenette PS, Fujisaki J. CD150(high) Bone Marrow Tregs Maintain Hematopoietic Stem Cell Quiescence and Immune Privilege via Adenosine. Cell Stem Cell. 2018 Mar 1;22(3):445-453.e5. eng. Declaration of Interests The authors have declared that no conflicting interests exist. Epub 20180215. doi:10.1016/j.stem.2018.01.017. Cited in: Pubmed; PMID 29456159.

20. Pačes J, Grobárová V, Zadražil Z, Knížková K, Malinská N, Tušková L, Boes M, Černý J. MHC II-EGFP Knock-in Mouse Model. Curr Protoc. 2023 Nov;3(11):e925. eng. doi:10.1002/cpz1.925. Cited in: Pubmed; PMID 37934124.

21. Boes M, Cerny J, Massol R, Op den Brouw M, Kirchhausen T, Chen J, Ploegh HL. T-cell engagement of dendritic cells rapidly rearranges MHC class II transport. Nature. 2002 Aug 29;418(6901):983-8. eng. doi:10.1038/nature01004. Cited in: Pubmed; PMID 12198548.

22. Heazlewood SY, Ahmad T, Cao B, Cao H, Domingues M, Sun X, Heazlewood CK, Li S, Williams B, Fulton M, White JF, Nebl T, Nefzger CM, Polo JM, Kile BT, Kraus F, Ryan MT, Sun YB, Choong PFM, Ellis SL, Anko ML, Nilsson SK. High ploidy large cytoplasmic megakaryocytes are hematopoietic stem cells regulators and essential for platelet production. Nat Commun. 2023 Apr 13;14(1):2099. eng. The authors declare no competing interests. Epub 20230413. doi:10.1038/s41467-023-37780-7. Cited in: Pubmed; PMID 37055407.

23. Zufferey A, Speck ER, Machlus KR, Aslam R, Guo L, McVey MJ, Kim M, Kapur R, Boilard E, Italiano JE, Jr., Semple JW. Mature murine megakaryocytes present antigen-MHC class I molecules to T cells and transfer them to platelets. Blood Adv. 2017 Sep 12;1(20):1773-1785. eng. Conflict-of-interest disclosure: The authors declare no competing financial interests. Epub 20170908. doi:10.1182/bloodadvances.2017007021. Cited in: Pubmed; PMID 29296823.

24. Blum JS, Wearsch PA, Cresswell P. Pathways of antigen processing. Annu Rev Immunol. 2013;31:443-73. eng. Epub 20130103. doi:10.1146/annurev-immunol-032712-095910. Cited in: Pubmed; PMID 23298205.

25. Pishesha N, Harmand TJ, Ploegh HL. A guide to antigen processing and presentation. Nat Rev Immunol. 2022 Dec;22(12):751-764. eng. Epub 20220413. doi:10.1038/s41577-022-00707-2. Cited in: Pubmed; PMID 35418563.

26. Li J, Williams MJ, Park HJ, Bastos HP, Wang X, Prins D, Wilson NK, Johnson C, Sham K, Wantoch M, Watcham S, Kinston SJ, Pask DC, Hamilton TL, Sneade R, Waller AK, Ghevaert C, Vassiliou GS, Laurenti E, Kent DG, Göttgens B, Green AR. STAT1 is essential for HSC function and maintains MHCIIhi stem cells that resist myeloablation and neoplastic expansion. Blood. 2022 Oct 6;140(14):1592-1606. eng. Conflict-of-interest disclosure: The authors declare no competing financial interests. doi:10.1182/blood.2021014009. Cited in: Pubmed; PMID 35767701.

27. Gollomp K, Poncz M. Gp1ba-Cre or Pf4-Cre: pick your poison. Blood. 2019 Jan 24;133(4):287-288. eng. Conflict-of-interest disclosure: The authors declare no competing financial interests. doi:10.1182/blood-2018-11-887513. Cited in: Pubmed; PMID 30679234.

28. Spindler M, Mott K, Schulze H, Bender M. Rapid isolation of mature murine primary megakaryocytes by size exclusion via filtration. Platelets. 2023 Dec;34(1):2192289. eng. doi:10.1080/09537104.2023.2192289. Cited in: Pubmed; PMID 36992536.

29. Yang Y, Liu Q, Zhang L, Fu X, Chen J, Hong D. A modified tape transfer approach for rapidly preparing high-quality cryosections of undecalcified adult rodent bones. J Orthop Translat. 2021 Jan;26:92-100. eng. The authors have no conflicts of interest to disclose in relation to this article. Epub 20200331. doi:10.1016/j.jot.2020.03.001. Cited in: Pubmed; PMID 33437628.

Acknowledgments

We would like to acknowledge Dr. Robert Welner and Dr. Jarrod Dudakov for their helpful and insightful conversations.

Funding:

National Institutes of Health National Institute of Diabetes and Digestive and Kidney Diseases R01DK139341 (KRM)

National Institutes of Health National Institute of Diabetes and Digestive and Kidney Diseases R21DK142111 (KRM)

National Institutes of Health National Heart, Lung, and Blood Institute R01HL151494 (KRM)

National Institutes of Health National Heart, Lung, and Blood Institute K99HL175037 (MNB)

National Institutes of Health National Heart, Lung, and Blood Institute R35HL161175 (JEI)

American Society of Hematology Restart Award (MNB)

American Society of Hematology Scholar Award (VC)

American Heart Association 24IPA1274573 (KRM)
American Heart Association 23POST1011433 (MNB)
American Heart Association 25DIVSUP1476419 (VC)

Author contributions:
Conceptualization: VC, KRM
Experimental Design: VC, KRM
Experimentation: VC, KGW, EC, ICB, DHL, JM, MC
Data Analysis: VC, MF, JM
Statistics: VC
Funding acquisition: VC, UvA, JEI, KRM
Supervision: JEI, KRM
Writing – original draft: VC, KRM
Writing – editing: VC, KRM, MB, EC, PH

Competing interests: JEI has a financial interest in and is a founder of StellularBio, a biotechnology company focused on making donor-independent platelet-like cells at scale. JEI has a financial interest in and is a founder of SpryBio, a biotechnology company focused on using shelf-stable platelets to treat osteoarthritis. Boston Children's Hospital manages the interests of JEI.

Data and materials availability: All data, code, and materials used in the analysis will be available upon reasonable request made to the corresponding author.